

Reproducing the Acoustic Velocity Vectors in a Spherical Listening Region

Jiarui Wang*, Thushara Abhayapala*, Jihui Aimee Zhang†, Prasanga Samarasinghe*

**The Australian National University* †*University of Southampton*

July 2023

Abstract

Acoustic velocity vectors are related to the human's perception of sound at low frequencies and have been widely used in Ambisonics. This paper proposes a spatial sound field reproduction algorithm based on matching the acoustic velocity vectors in the spherical listening region. Using the sound field translation formula, the spherical harmonic coefficients of the acoustic velocity vectors in the spherical listening region are derived from the spherical harmonic coefficients of the pressure, which can be measured by a higher-order microphone array. Unlike previous work in which the acoustic velocity vectors are only controlled on the boundary of the listening region or at discrete sweet spots, this work directly manipulates the acoustic velocity vectors in the whole spherical listening region, which allows the listener to move beyond the sweet spots. Simulations show the proposed reproduction algorithm can accurately reproduce the acoustic velocity vectors in the spherical listening region, with better performance at low frequencies.

1 Introduction

Spatial sound field reproduction aims to synthesize the desired sound field in the listening region. In most cases, the sound field is characterized by the pressure. Pressure based methods include matching the pressure at a number of sweet spots [1], wave field synthesis [2–6] and higher order Ambisonics [7–9]. However, a higher accuracy in reproduced pressure does not guarantee satisfactory perception [10].

Acoustic velocity vectors are related to human's perception of sound at low frequencies [11, 12] and have been applied to reproduction at sweet spots. In [13], acoustic velocity vectors were used in the ba-

sic Ambisonic decoding to reproduce the impression of the original sound at frequencies below 500 Hz. Gerzon also claimed that acoustic velocity vectors are essential to the localization at frequencies below 700 Hz [11] and proposed the r_V vector used in Ambisonics [11, 12, 14]. A time-domain method that jointly controls the acoustic velocity vectors and the pressures at multiple sweet spots was derived in [15]. To ensure the listeners can move beyond the sweet spots, the acoustic velocity vectors in the whole listening region should be characterized.

Based on the concept of boundary control, a reproduction method based on matching the acoustic velocity vectors at discrete control points on the boundary of the listening region was proposed in [16]. Similar ideas were proposed in [17] and [18], where the pressures and the acoustic velocity vectors were controlled on the boundaries of multiple listening zones. Measuring the acoustic velocity vectors at multiple control points involves a complicated setup. Moreover, the methods in [17] and [18] require a large number of loudspeakers, which may not be suitable for home theatre or small exhibition space.

In [19], the spherical harmonic (SH) coefficients of the acoustic velocity vectors (abbrev. **SHV** coefficients) in a spherical region were derived from the SH coefficients of the pressure, which can be obtained by a spherical microphone array [20, 21]. The need of measuring the acoustic velocity vectors at multiple control points was eliminated. The SHV coefficients in [19] are of the form $X_a^d(k, r_b)$, which has an inseparable radial component r_b . To cover a spherical region, the SHV coefficients must be calculated for different radii.

To characterize the acoustic velocity vectors in a spherical listening region using one set of SH coefficients across all radii, this paper presents the SHV coefficients independent of the radial distance

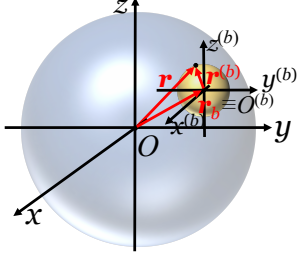


Figure 1: Setup of the geometric model. The listening region is in light blue. \mathbf{r}_b is a point in the listening region.

(abbrev. **SHV-indR** coefficients). The SHV-indR coefficients are of the form $(\zeta_{\hat{\epsilon}}^d)_a^d(k)$ and the radial dependency is captured by a separate radial function $R_a(kr_b)$. Starting from the definition of the acoustic velocity vectors, it is found that the SHV-indR coefficients are related to the SH coefficients of the pressure by the sound field translation formula. Therefore, the SHV-indR coefficients retain the benefit that they can be derived from spherical microphone array measurements. In [22], the SHV-indR coefficients were derived by using eigenbeam-ESPRIT, which is a source localization method. For an example application, this paper shows that the SHV-indR coefficients can be used in spatial sound field reproduction system to reproduce the acoustic velocity vectors in the whole spherical listening region.

2 Acoustic velocity vectors in the spherical region

2.1 Setup of the geometric model

Figure 1 shows the setup of the geometric model. The spherical listening region in light blue is free from sources and scatterers. The derivation starts from finding the acoustic velocity vectors at \mathbf{r}_b , which could be any points within the listening region. The local $x^{(b)}y^{(b)}z^{(b)}$ coordinate system is centered at $\mathbf{r}_b \equiv O^{(b)}$. The $x^{(b)}y^{(b)}z^{(b)}$ coordinate system is the translation of the xyz coordinate system with \mathbf{r}_b as the translation vector. Note that $\mathbf{r} = \mathbf{r}_b + \mathbf{r}^{(b)}$. In this paper, the superscript indicates the coordinate system used to express the location. If there are no superscripts, then the location is expressed with respect to the xyz coordinate system.

2.2 Acoustic velocity vectors at a point

In Figure 1, the pressure at a point $\mathbf{r}^{(b)} \equiv (r^{(b)}, \theta^{(b)}, \phi^{(b)})$ within the local region in yellow is

$$p(k, \mathbf{r}^{(b)}) = \sum_{n=0}^N \sum_{m=-n}^n \beta_n^m(k, \mathbf{r}_b) j_n(kr^{(b)}) Y_n^m(\theta^{(b)}, \phi^{(b)}) \quad (1)$$

in which k is the wavenumber, $j_n(\cdot)$ is the spherical Bessel function of the first kind, $Y_n^m(\cdot, \cdot)$ is the SH function of degree n and order m , and N is the truncation order. The SH coefficients $\beta_n^m(k, \mathbf{r}_b)$ depend on the location of \mathbf{r}_b , which is the origin of the local coordinate system. From [23],

$$\left. \frac{\partial j_n(kr^{(b)})}{\partial r^{(b)}} \right|_{r^{(b)}=0} = \frac{1}{3} k \delta_{n,1} \quad (2)$$

in which $\delta_{n,1}$ is the Kronecker delta function.

Let ρ_0 denote the density of the medium and c denote the speed of sound. Let $\hat{\mathbf{x}}$, $\hat{\mathbf{y}}$ and $\hat{\mathbf{z}}$ denote the unit vectors along the x, y, z axes. The acoustic velocity vectors at $\mathbf{r}_b \equiv O^{(b)}$ are the linear combinations of the first order SH coefficients of the pressure and can be written as [24]

$$\begin{aligned} V_{\hat{\mathbf{x}}}(\mathbf{r}_b, k) &= \frac{i}{k\rho_0 c} \left. \frac{\partial p(k, \mathbf{r}^{(b)})}{\partial x} \right|_{r^{(b)}=0} \\ &= \sum_{n=0}^N \sum_{m=-n}^n \beta_n^m(k, \mathbf{r}_b) \left. \frac{\partial j_n(kr^{(b)})}{\partial r^{(b)}} \right|_{r^{(b)}=0} Y_n^m\left(\frac{\pi}{2}, 0\right) \\ &= \frac{1}{3} \frac{i}{\rho_0 c} \left[\sqrt{\frac{3}{8\pi}} \beta_1^{-1}(k, \mathbf{r}_b) - \sqrt{\frac{3}{8\pi}} \beta_1^1(k, \mathbf{r}_b) \right], \quad (3) \end{aligned}$$

$$\begin{aligned} V_{\hat{\mathbf{y}}}(\mathbf{r}_b, k) &= \frac{i}{k\rho_0 c} \left. \frac{\partial p(k, \mathbf{r}^{(b)})}{\partial y} \right|_{r^{(b)}=0} \\ &= \sum_{n=0}^N \sum_{m=-n}^n \beta_n^m(k, \mathbf{r}_b) \left. \frac{\partial j_n(kr^{(b)})}{\partial r^{(b)}} \right|_{r^{(b)}=0} Y_n^m\left(\frac{\pi}{2}, \frac{\pi}{2}\right) \\ &= \frac{1}{3} \frac{i}{\rho_0 c} \left[-\sqrt{\frac{3}{8\pi}} i \beta_1^{-1}(k, \mathbf{r}_b) - \sqrt{\frac{3}{8\pi}} i \beta_1^1(k, \mathbf{r}_b) \right], \quad (4) \end{aligned}$$

$$\begin{aligned} V_{\hat{\mathbf{z}}}(\mathbf{r}_b, k) &= \frac{i}{k\rho_0 c} \left. \frac{\partial p(k, \mathbf{r}^{(b)})}{\partial z} \right|_{r^{(b)}=0} \\ &= \sum_{n=0}^N \sum_{m=-n}^n \beta_n^m(k, \mathbf{r}_b) \left. \frac{\partial j_n(kr^{(b)})}{\partial r^{(b)}} \right|_{r^{(b)}=0} Y_n^m(0, 0) \\ &= \frac{1}{3} \frac{i}{\rho_0 c} \sqrt{\frac{3}{4\pi}} \beta_1^0(k, \mathbf{r}_b). \quad (5) \end{aligned}$$

2.3 Acoustic velocity vectors in the spherical region

This paper aims to find the SH decomposition of the acoustic velocity vectors such that

$$V_{\hat{\mathbf{e}}}(\mathbf{r}_b, k) = \sum_{a=0}^A \sum_{d=-a}^a (\zeta_{\hat{\mathbf{e}}}_a^d(k) R_a(kr_b) Y_a^d(\theta_b, \phi_b)) \quad (6)$$

in which $\hat{\mathbf{e}} \in \{\hat{\mathbf{x}}, \hat{\mathbf{y}}, \hat{\mathbf{z}}\}$, $R_a(kr_b)$ denotes the radial function, A is the truncation order, and $(\zeta_{\hat{\mathbf{e}}}_a^d(k))$ are the SHV-indR coefficients. Since $\beta_1^m(k, \mathbf{r}_b)$ with $m \in \{-1, 0, 1\}$ are functions of $\mathbf{r}_b \equiv (r_b, \theta_b, \phi_b)$, it is possible to write

$$\beta_1^m(k, \mathbf{r}_b) = \sum_{a=0}^A \sum_{d=-a}^a (\gamma_1^m)_a^d(k) R_a(kr_b) Y_a^d(\theta_b, \phi_b). \quad (7)$$

From (3), (4) and (5),

$$(\zeta_{\hat{\mathbf{x}}}_a^d(k)) = \frac{1}{3} \frac{i}{\rho_0 c} \left[\sqrt{\frac{3}{8\pi}} (\gamma_1^{-1})_a^d(k) - \sqrt{\frac{3}{8\pi}} (\gamma_1^1)_a^d(k) \right], \quad (8)$$

$$(\zeta_{\hat{\mathbf{y}}}_a^d(k)) = \frac{1}{3} \frac{i}{\rho_0 c} \left[-\sqrt{\frac{3}{8\pi}} i (\gamma_1^{-1})_a^d(k) - \sqrt{\frac{3}{8\pi}} i (\gamma_1^1)_a^d(k) \right], \quad (9)$$

$$(\zeta_{\hat{\mathbf{z}}}_a^d(k)) = \frac{1}{3} \frac{i}{\rho_0 c} \sqrt{\frac{3}{4\pi}} (\gamma_1^0)_a^d(k). \quad (10)$$

Now the goal is to find $(\gamma_1^m)_a^d(k)$. In Figure 1, the pressure at $\mathbf{r} \equiv (r, \theta, \phi)$ is

$$p(k, \mathbf{r}) = \sum_{\ell=0}^L \sum_{q=-\ell}^{\ell} \xi_{\ell}^q(k) j_{\ell}(kr) Y_{\ell}^q(\theta, \phi). \quad (11)$$

in which $\xi_{\ell}^q(k)$ are the SH coefficients of the global pressure, and L is the truncation order. Using the sound field translation formula [25],

$$p(k, \mathbf{r}^{(b)}) = \sum_{n=0}^N \sum_{m=-n}^n \underbrace{\sum_{a=0}^A \sum_{\ell=0}^L \sum_{q=-\ell}^{\ell} \xi_{\ell}^q(k) G_{nm}^{\ell qa} j_a(kr_b) Y_a^{(q-m)}(\theta_b, \phi_b)}_{\beta_n^m(k, \mathbf{r}_b) \text{ in (1)}}$$

$$j_n(kr^{(b)}) Y_n^m(\theta^{(b)}, \phi^{(b)}). \quad (12)$$

Since the acoustic velocity vectors involve only the first order SH coefficients, the derivation restricts $n = 1$ and $m = \{-1, 0, 1\}$. The term

$$G_{1m}^{\ell qa} = 4\pi i^{1+a-\ell} (-1)^q \sqrt{\frac{3(2\ell+1)(2a+1)}{4\pi}} W_1 W_2 \quad (13)$$

in which W_1 and W_2 are the Wigner-3j symbols

$$W_1 = \begin{pmatrix} \ell & 1 & a \\ 0 & 0 & 0 \end{pmatrix} \quad W_2 = \begin{pmatrix} \ell & 1 & a \\ -q & m & q-m \end{pmatrix}. \quad (14)$$

Let $d = q - m$, $\beta_1^m(k, \mathbf{r}_b)$ in (12) becomes

$$\begin{aligned} \beta_1^m(k, \mathbf{r}_b) &= \sum_{a=0}^A \sum_{\ell=0}^L \sum_{d=-\ell-m}^{\ell-m} \xi_{\ell}^{(d+m)}(k) G_{1m}^{\ell(d+m)a} j_a(kr_b) Y_a^d(\theta_b, \phi_b) \\ &= \sum_{a=0}^A \sum_{d=-L-m}^{L-m} \underbrace{\left[\sum_{\ell=|d+m|}^L \xi_{\ell}^{(d+m)}(k) G_{1m}^{\ell(d+m)a} \right]}_{(\gamma_1^m)_a^d \text{ in (7)}} \\ &\quad j_a(kr_b) Y_a^d(\theta_b, \phi_b). \end{aligned} \quad (15)$$

Comparing (15) and (7), the radial function in (7) (and hence in (6)) satisfies $R_a(kr_b) = j_a(kr_b)$.

Operator matrices can be constructed to link the SH coefficients $\xi_{\ell}^{(d+m)}(k)$ of the global pressure to $(\gamma_1^m)_a^d(k)$ with $m \in \{-1, 0, 1\}$ such that

$$(\gamma_1^m)(k) = \mathfrak{B}_1^m \boldsymbol{\xi}(k) \quad (16)$$

in which $(\gamma_1^m)(k)$ and $\boldsymbol{\xi}(k)$ are the column vectors formed by concatenating $(\gamma_1^m)_a^d(k)$ and $\xi_{\ell}^{(d+m)}(k)$, respectively. The operator matrices do not depend on the wavenumber k (also the frequency) because $G_{1m}^{\ell(d+m)a}$ are frequency independent.

The calculation of \mathfrak{B}_1^m does not require significant resources because only three operator matrices with $m = \{-1, 0, 1\}$ are required. Moreover, $G_{1m}^{\ell(d+m)a}$ is non-zero only when $|\ell-1| \leq a \leq \ell+1$. Furthermore, since $W_1 = 0$ when $a = \ell$, only two conditions $a = |\ell-1|$ and $a = \ell+1$ need to be considered. The dimension of \mathfrak{B}_1^m is L^2 by $(L+1)^2$. This is because if $\xi_{\ell}^{(d+m)}(k)$ is measured up to degree L , the maximum degree of $(\gamma_1^m)_a^d(k)$ can be calculated is $(L-1)$. For $a = L$, $\xi_{\ell}^{(d+m)}(k)$ with $\ell = L+1$ should be measured.

Operator matrices $\mathfrak{B}_{\hat{\mathbf{e}}}$ with $\hat{\mathbf{e}} \in \{\hat{\mathbf{x}}, \hat{\mathbf{y}}, \hat{\mathbf{z}}\}$ that directly link the SHV-indR coefficients $(\zeta_{\hat{\mathbf{e}}}_a^d(k))$ and the SH coefficients $\xi_{\ell}^{(d+m)}(k)$ of the global pressure are constructed so that

$$\boldsymbol{\zeta}_{\hat{\mathbf{e}}}(k) = \mathfrak{B}_{\hat{\mathbf{e}}} \boldsymbol{\xi}(k) \quad (17)$$

in which $\boldsymbol{\zeta}_{\hat{\mathbf{e}}}(k)$ is the column vector formed by con-

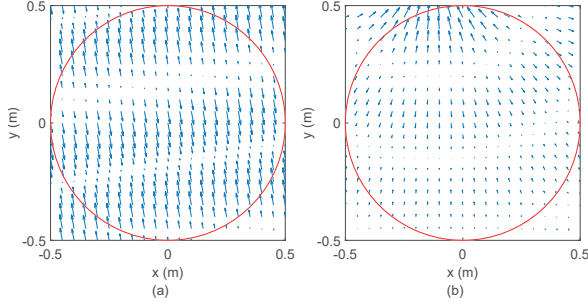


Figure 2: Real part of the acoustic velocity vectors on the xy plane at 500 Hz. (a) A plane wave with incident direction $(\theta_{pw}, \phi_{pw}) = (\pi/2, 1.745)$ rad. (b) A point source at $\mathbf{r}_{ps} = (0.7 \text{ m}, \pi/2 \text{ rad}, 1.745 \text{ rad})$.

catenating $(\zeta_{\hat{e}}^d)_a(k)$. From (8), (9) and (10),

$$\mathfrak{B}_{\hat{x}} = \frac{1}{3} \frac{i}{\rho_0 c} \left[\sqrt{\frac{3}{8\pi}} \mathfrak{B}_1^{-1} - \sqrt{\frac{3}{8\pi}} \mathfrak{B}_1^1 \right], \quad (18)$$

$$\mathfrak{B}_{\hat{y}} = \frac{1}{3} \frac{i}{\rho_0 c} \left[-\sqrt{\frac{3}{8\pi}} i \mathfrak{B}_1^{-1} - \sqrt{\frac{3}{8\pi}} i \mathfrak{B}_1^1 \right], \quad (19)$$

$$\mathfrak{B}_{\hat{z}} = \frac{1}{3} \frac{i}{\rho_0 c} \sqrt{\frac{3}{4\pi}} \mathfrak{B}_1^0. \quad (20)$$

2.4 Illustration of the acoustic velocity vectors in a spherical region

This subsection illustrates the acoustic velocity vectors in a spherical listening region due to a plane wave and a point source. For a plane wave with incident direction (θ_{pw}, ϕ_{pw}) ,

$$\xi_\ell^q(k) = 4\pi i^\ell \overline{Y_\ell^q(\theta_{pw}, \phi_{pw})} \quad \forall k. \quad (21)$$

in which $\overline{(\cdot)}$ denotes conjugation. For a point source located at $\mathbf{r}_{ps} \equiv (r_{ps}, \theta_{ps}, \phi_{ps})$,

$$\xi_\ell^q(k) = -ik h_\ell^{(2)}(kr_{ps}) \overline{Y_\ell^q(\theta_{ps}, \phi_{ps})} \quad (22)$$

in which $h_\ell^{(2)}(\cdot)$ is the spherical Hankel function of the second kind.

Figure 2(a) shows the real part of the acoustic velocity vectors on the xy plane due to a plane wave with incident direction $(\theta_{pw}, \phi_{pw}) = (\pi/2, 1.745)$ rad, whereas Figure 2(b) shows the real part of the acoustic velocity vectors on the xy plane due to a point source located at $\mathbf{r}_{ps} = (0.7 \text{ m}, \pi/2 \text{ rad}, 1.745 \text{ rad})$. The listening region bounded by the red circle is of radius 0.5 meters and the frequency is at 500 Hz. The global pressure SH coefficients are truncated to $L = 7$ and the SHV-indR coefficients are truncated to $A = 6$. In Figure 2(a), the directions of the acoustic velocity vectors

are either parallel or anti-parallel. This is because for a plane wave, the acoustic velocity vectors are perpendicular to the wave front. In Figure 2(b), the acoustic velocity vectors either converge to or diverge from a point in the direction of $\phi = 1.745$ rad. This is because the wave fronts of a point source are spherical.

3 Reproducing the acoustic velocity vectors in a spherical region

This section presents the sound field reproduction simulation based on matching the SHV-indR coefficients in the spherical listening region. Assume there are S number of loudspeakers. First, the SH coefficients $(\xi^{\text{des}})_\ell^q(k)$ of the desired global pressure are calculated or measured by a spherical microphone array. Next, using the operator matrices in (17), the desired SHV-indR coefficients $(\zeta_{\hat{e}}^{\text{des}})_a^d(k)$ with $\hat{e} \in \{\hat{x}, \hat{y}, \hat{z}\}$ are calculated. Then, the SH coefficients $(\xi^{\text{L}s})_\ell^q(k)$ of the global pressure due to unit output from the s -th loudspeaker with $s = 1, 2, \dots, S$ are measured. After that, using (17), the SHV-indR coefficients $(\zeta_{\hat{e}}^{\text{L}s})_a^d(k)$ with $\hat{e} \in \{\hat{x}, \hat{y}, \hat{z}\}$ due to unit output from the s -th loudspeaker are found. Finally, a system of equation can be established

$$\zeta^{\text{des}}(k) = \mathbf{H}(k) \mathbf{w}(k). \quad (23)$$

In (23), $\zeta^{\text{des}}(k) = [\zeta_{\hat{x}}^{\text{des}}(k)^T, \zeta_{\hat{y}}^{\text{des}}(k)^T, \zeta_{\hat{z}}^{\text{des}}(k)^T]^T$ in which $\zeta_{\hat{e}}^{\text{des}}(k)$ with $\hat{e} \in \{\hat{x}, \hat{y}, \hat{z}\}$ is the column vector formed by concatenating $(\zeta_{\hat{e}}^{\text{des}})_a^d(k)$ and $(\cdot)^T$ denotes matrix transpose. The matrix $\mathbf{H}(k) = [\zeta^{\text{L}1}(k), \zeta^{\text{L}2}(k), \dots, \zeta^{\text{L}S}(k)]$ and its s -th column $\zeta^{\text{L}s}(k) = [\zeta_{\hat{x}}^{\text{L}s}(k)^T, \zeta_{\hat{y}}^{\text{L}s}(k)^T, \zeta_{\hat{z}}^{\text{L}s}(k)^T]^T$ in which $\zeta_{\hat{e}}^{\text{L}s}(k)$ is the column vector formed by concatenating $(\zeta_{\hat{e}}^{\text{L}s})_a^d(k)$ with $\hat{e} \in \{\hat{x}, \hat{y}, \hat{z}\}$. The column vector $\mathbf{w}(k)$ contains the weight (also called driving function) of each loudspeaker. The weights are solved by using Moore-Penrose pseudoinverse. The velocity based method is compared with the pressure based method, which finds the loudspeaker weights by matching the SH coefficients of the global pressure. Like (23), the system of equation for the pressure based method is

$$\xi^{\text{des}}(k) = \mathbf{G}(k) \mathbf{w}(k) \quad (24)$$

in which $\xi^{\text{des}}(k)$ is the column vector formed by concatenating $(\xi^{\text{des}})_\ell^q(k)$. The matrix $\mathbf{G}(k) =$

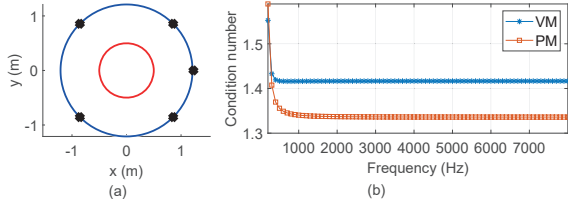


Figure 3: (a) Setup of the reproduction system. The listening region of radius 0.5 meters is bounded by the red circle. The loudspeakers are denoted by black crosses. (b) Condition numbers of $\mathbf{H}(k)$ (VM) and $\mathbf{G}(k)$ (PM).

$[\xi^{\text{L1}}(k), \xi^{\text{L2}}(k), \dots, \xi^{\text{LS}}(k)]$ in which the s -th column $\xi^{\text{LS}}(k)$ is formed by concatenating $(\xi^{\text{LS}})^q(k)$. The loudspeaker weights $\mathbf{w}(k)$ are found by Moore-Penrose pseudoinverse.

Figure 3(a) shows the simulation setup. The five loudspeakers are located on a circle of radius 1.21 meters. The azimuth angles of the loudspeakers are $[0, \pi/4, 3\pi/4, 5\pi/4, 7\pi/4]$ rad. The loudspeakers are assumed to be point sources. The listening region is bounded by the red circle with radius 0.5 meters. The desired sound field is a plane wave with incident direction $(\theta_{\text{pw}}, \phi_{\text{pw}}) = (\pi/2, 1.745)$ rad. The SH coefficients of the pressure $\xi_\ell^q(k)$ are truncated to $\ell = 4$ and as a consequence, the SHV-indR coefficients $(\zeta_{\hat{e}}^d)_a(k)$ are truncated to $a = 3$. At each wavenumber k , the dimension of $\mathbf{H}(k)$ is 48-by-5 and the dimension of $\mathbf{G}(k)$ is 25-by-5. Figure 3(b) shows the condition numbers of $\mathbf{H}(k)$ in (23) and $\mathbf{G}(k)$ in (24). The condition numbers remain stable, though those of $\mathbf{H}(k)$ are slightly greater than those of $\mathbf{G}(k)$. The Moore-Penrose pseudoinverse is calculated by the `pinv` function in MATLAB and the default tolerance is used. Future work should consider finding a more appropriate tolerance value.

Figure 4 shows the reproduced pressure and the acoustic velocity vectors on the xy plane at 500 Hz. Figures 4(a) and 4(c) are from the velocity based method proposed in this paper, whereas Figures 4(b) and 4(d) are from the pressure based method. The ground truth of the acoustic velocity vectors is in Figure 2(a). The velocity based method achieves better results in both reproduced pressure and reproduced velocity. Like [26] and [27], the velocity reproduction error

$$\eta(k) = \cos^{-1}(\text{DOT}(k))/\pi \quad (25)$$

with

$$\text{DOT}(k) = \frac{\mathbf{V}^{\text{des}}(\mathbf{r}_b, k)}{\|\mathbf{V}^{\text{des}}(\mathbf{r}_b, k)\|_2} \cdot \frac{\mathbf{V}^{\text{re}}(\mathbf{r}_b, k)}{\|\mathbf{V}^{\text{re}}(\mathbf{r}_b, k)\|_2} \quad (26)$$

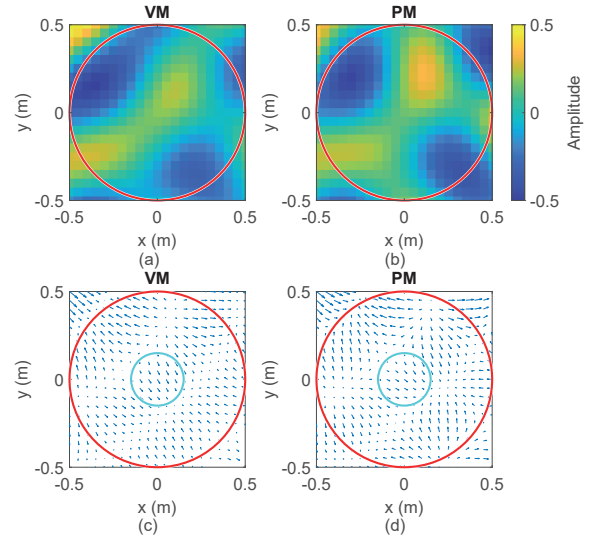


Figure 4: Real part of the reproduced pressure and the reproduced acoustic velocity vectors on the xy plane at 500 Hz. The desired sound field is a plane wave with incident direction $(\pi/2, 1.745)$ rad. (a) and (c) - velocity based method (VM); (b) and (d) - pressure based method (PM).

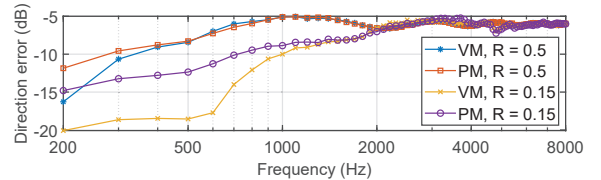


Figure 5: Velocity reproduction errors in the real part of the reproduced acoustic velocity vectors. VM - velocity based method; PM - pressure based method.

in which $\mathbf{V}^{\text{des}}(\mathbf{r}_b, k) \equiv [V_{\hat{x}}^{\text{des}}(\mathbf{r}_b, k), V_{\hat{y}}^{\text{des}}(\mathbf{r}_b, k), V_{\hat{z}}^{\text{des}}(\mathbf{r}_b, k)]$ is the desired acoustic velocity vector and $\mathbf{V}^{\text{re}}(\mathbf{r}_b, k) \equiv [V_{\hat{x}}^{\text{re}}(\mathbf{r}_b, k), V_{\hat{y}}^{\text{re}}(\mathbf{r}_b, k), V_{\hat{z}}^{\text{re}}(\mathbf{r}_b, k)]$ is the reproduced acoustic velocity vector. Here, only the real part of the acoustic velocity vectors are considered. Figure 5 shows the velocity reproduction errors on the 2D plane. The blue line and the red line illustrate the velocity reproduction errors averaged across 2821 evaluation points within the red circle in Figure 3(a). The velocity based method achieved lower errors below 500 Hz. Above 500 Hz, the errors of the velocity based method and the pressure based method are similar. The yellow line and the purple line show the velocity reproduction errors averaged across 249 evaluation points within the cyan circle of radius 0.15 meters located at the center of the listening region. Up to 1 kHz, the velocity based method performs better than the pressure based method. Since human's perception of sound is related to the acoustic velocity vectors

at low frequencies [11, 12], the velocity based method could result in improved perception when the listener is in the vicinity of the center of the listening region. For reproduction at mid to high frequencies, intensity based method [13, 27–30] can be used. Note that the reproduction error will be different when the desired plane wave is coming from a different direction.

4 Conclusion

This paper presented the SHV-indR coefficients, which are the SH coefficients of the acoustic velocity vectors in a spherical region independent of the radial distance. The SHV-indR coefficients were derived from spherical microphone array measurements of the pressure by using the sound field translation formula. The SHV-indR coefficients were used in sound field reproduction system to reproduce the acoustic velocity vectors in the spherical listening region, with better performance achieved at low frequencies. Future work will include conducting perceptual tests and investigating methods to enlarge the listening region.

References

- [1] O. Kirkeby and P. A. Nelson, “Reproduction of plane wave sound fields,” *The Journal of the Acoustical Society of America*, vol. 94, no. 5, pp. 2992–3000, 11 1993.
- [2] A. J. Berkhout, D. de Vries, and P. Vogel, “Acoustic control by wave field synthesis,” *The Journal of the Acoustical Society of America*, vol. 93, no. 5, pp. 2764–2778, 05 1993.
- [3] M. M. Boone, E. N. G. Verheijen, and P. F. van Tol, “Spatial sound-field reproduction by wave-field synthesis,” *Journal of the Audio Engineering Society*, vol. 43, no. 12, pp. 1003–1012, December 1995.
- [4] J. Ahrens, R. Rabenstein, and S. Spors, “The theory of wave field synthesis revisited,” *Journal of the Audio Engineering Society*, May 2008.
- [5] P.-A. Gauthier and A. Berry, “Adaptive wave field synthesis for active sound field reproduction: Experimental results,” *The Journal of the Acoustical Society of America*, vol. 123, no. 4, pp. 1991–2002, 04 2008.
- [6] F. Winter, F. Schultz, G. Firtha, and S. Spors, “A geometric model for prediction of spatial aliasing in 2.5 D sound field synthesis,” *IEEE/ACM Transactions on Audio, Speech, and Language Processing*, vol. 27, no. 6, pp. 1031–1046, 2019.
- [7] D. Ward and T. Abhayapala, “Reproduction of a plane-wave sound field using an array of loudspeakers,” *IEEE Transactions on Speech and Audio Processing*, vol. 9, no. 6, pp. 697–707, 2001.
- [8] T. Betlehem and T. D. Abhayapala, “Theory and design of sound field reproduction in reverberant rooms,” *The Journal of the Acoustical Society of America*, vol. 117, no. 4, pp. 2100–2111, 04 2005.
- [9] M. A. Poletti, “Three-dimensional surround sound systems based on spherical harmonics,” *Journal of the Audio Engineering Society*, vol. 53, no. 11, pp. 1004–1025, November 2005.
- [10] S. Spors, H. Wierstorf, A. Raake, F. Melchior, M. Frank, and F. Zotter, “Spatial sound with loudspeakers and its perception: A review of the current state,” *Proceedings of the IEEE*, vol. 101, no. 9, pp. 1920–1938, 2013.
- [11] M. A. Gerzon and G. J. Barton, “Ambisonic decoders for HDTV,” in *Audio Engineering Society Convention 92*, Mar 1992.
- [12] M. A. Gerzon, “General metatheory of auditory localisation,” in *Audio Engineering Society Convention 92*, Mar 1992.
- [13] D. Arteaga, “An ambisonics decoder for irregular 3D loudspeaker arrays,” in *The 134th AES Convention*, 01 2013.
- [14] F. Zotter and M. Frank, *Ambisonics: A Practical 3D Audio Theory for Recording, Studio Production, Sound Reinforcement, and Virtual Reality*. Springer, 2019.
- [15] X. Hu, J. Wang, W. Zhang, and L. Zhang, “Time-domain sound field reproduction with pressure and particle velocity jointly controlled,” *Applied Sciences*, vol. 11, no. 22, 2021.

- [16] M. Shin, P. A. Nelson, F. M. Fazi, and J. Seo, “Velocity controlled sound field reproduction by non-uniformly spaced loudspeakers,” *Journal of Sound and Vibration*, vol. 370, pp. 444–464, 2016.
- [17] M. Buerger, R. Maas, H. W. Löllmann, and W. Kellermann, “Multizone sound field synthesis based on the joint optimization of the sound pressure and particle velocity vector on closed contours,” in *2015 IEEE Workshop on Applications of Signal Processing to Audio and Acoustics (WASPAA)*, 2015, pp. 1–5.
- [18] M. Buerger, C. Hofmann, and W. Kellermann, “Broadband multizone sound rendering by jointly optimizing the sound pressure and particle velocity,” *The Journal of the Acoustical Society of America*, vol. 143, no. 3, pp. 1477–1490, 03 2018.
- [19] H. Zuo, T. D. Abhayapala, and P. N. Samarasinghe, “Particle velocity assisted three dimensional sound field reproduction using a modal-domain approach,” *IEEE/ACM Transactions on Audio, Speech, and Language Processing*, vol. 28, pp. 2119–2133, 2020.
- [20] J. Meyer and G. Elko, “A highly scalable spherical microphone array based on an orthonormal decomposition of the soundfield,” in *2002 IEEE International Conference on Acoustics, Speech, and Signal Processing*, vol. 2, 2002, pp. II–1781–II–1784.
- [21] T. D. Abhayapala and D. B. Ward, “Theory and design of high order sound field microphones using spherical microphone array,” in *2002 IEEE International Conference on Acoustics, Speech, and Signal Processing*, vol. 2, 2002, pp. II–1949–II–1952.
- [22] A. Herzog and E. A. P. Habets, “Generalized intensity vector and energy density in the spherical harmonic domain: Theory and applications,” *The Journal of the Acoustical Society of America*, vol. 150, no. 1, pp. 294–306, 07 2021.
- [23] F. Ma, T. D. Abhayapala, and W. Zhang, “Multiple circular arrays of vector sensors for real-time sound field analysis,” *IEEE/ACM Transactions on Audio, Speech, and Language Processing*, vol. 29, pp. 286–299, 2021.
- [24] A. H. Moore, C. Evers, and P. A. Naylor, “Direction of arrival estimation in the spherical harmonic domain using subspace pseudointensity vectors,” *IEEE/ACM Transactions on Audio, Speech, and Language Processing*, vol. 25, no. 1, pp. 178–192, 2017.
- [25] B. Rafaely, *Fundamentals of Spherical Array Processing*. Springer, 2015.
- [26] L. Birnie, T. Abhayapala, V. Tourbabin, and P. Samarasinghe, “Mixed source sound field translation for virtual binaural application with perceptual validation,” *IEEE/ACM Transactions on Audio, Speech, and Language Processing*, vol. 29, pp. 1188–1203, 2021.
- [27] H. Zuo, P. N. Samarasinghe, and T. D. Abhayapala, “Intensity based spatial soundfield reproduction using an irregular loudspeaker array,” *IEEE/ACM Transactions on Audio, Speech, and Language Processing*, vol. 28, pp. 1356–1369, 2020.
- [28] —, “Intensity based soundfield reproduction over multiple sweet spots using an irregular loudspeaker array,” in *2020 28th European Signal Processing Conference (EUSIPCO)*, 2021, pp. 486–490.
- [29] H. Zuo, T. D. Abhayapala, and P. N. Samarasinghe, “3d multizone soundfield reproduction in a reverberant environment using intensity matching method,” in *ICASSP 2021 - 2021 IEEE International Conference on Acoustics, Speech and Signal Processing (ICASSP)*, 2021, pp. 416–420.
- [30] J.-W. Choi and Y.-H. Kim, “Manipulation of sound intensity within a selected region using multiple sources,” *The Journal of the Acoustical Society of America*, vol. 116, no. 2, pp. 843–852, 08 2004.